HYCON3D for Thermal-Hydraulic Behavior in PWR Containment under Early and Late-Phase Severe Accident Conditions

Jongtae Kim [a*], Kukhee Lim [b], Eunho Kim [b]
[a] *Intelligent Accident Mitigation Reasearch Division, KAERI*
[b] *Department of Severe Accident and Risk Assessment, KINS, Gwahak-ro 62, Daejeon, Korea*
[*] *Corresponding author: ex-kjt@kaeri.re.kr*

Keywords : Nuclear Power Plant, 3D thermal-hydraulics, Severe Accident, Combustible Gas

1. Introduction

Lumped-parameter (LP)-based integrated analysis codes are widely used to predict the behavior and distribution of water vapor and combustible gases (e.g., hydrogen and carbon monoxide) released into the containment building during severe accidents. Representative codes such as MELCOR employ fundamental conservation equations combined with correlation-based models, enabling efficient computations with relatively low computational cost. These codes have been extensively applied to assess hydrogen safety in reactor containment buildings under severe accident conditions. However, the complex behavior of steam and combustible gases within containment during severe accidents is difficult to validate empirically, as full-scale experimental data are inherently limited. Consequently, the need for realistic best-estimate methodologies has become increasingly important. In this context, turbulence-resolved, multidimensional analysis codes are considered essential to complement LP-based integrated analysis tools.

The CONTAIN3D code [1] was developed to analyze hydrogen safety in nuclear power plant (NPP) containments during the early phase of severe accidents. It has been applied to investigate hydrogen behavior in a Korean typical high-power reactor containment up to reactor vessel failure under small-break loss-of-coolant accident (SBLOCA) and station blackout (SBO) scenarios [2].

In pressurized water reactors (PWRs), hydrogen mitigation systems (HMS) employing passive autocatalytic recombiners (PARs) are installed to control hydrogen concentration during design-basis accidents and early-phase severe accidents. Recent studies have indicated that PARs are also capable of recombining carbon monoxide (CO), which may be generated by molten corium–concrete interaction (MCCI) during the late phase of severe accidents. Since CO is a combustible gas similar to hydrogen, it must also be considered a potential flammability hazard within the containment.

Although experimental research on CO recombination by PARs is being conducted in several countries, most PAR vendors, except Framatome [3], have not yet provided reliable correlation models for CO removal performance. Furthermore, representative severe accident codes such as MELCOR [4] do not currently include a validated correlation model for CO recombination by PARs.

To address these limitations, the turbulence-resolved CFD code HYCON3D [5] has recently been developed based on CONTAIN3D to analyze thermal-hydraulic behavior in PWR containments during both early and late phases of severe accidents. In this study, the late phase refers to accident progression after reactor vessel failure, during which large amounts of steam and CO may be released into the containment.

This paper presents the analytical model implemented in HYCON3D for CO recombination and its validation results. In addition, simulation results for early and late phases of an SBO accident in the Korean typical high-power reactor containment are discussed.

2. Introduction of HYCON3D Code

The governing equations describing steam condensation, multicomponent gas diffusion, and turbulent thermo-fluid behavior with compressibility effects in the containment can be formulated in various forms depending on the modeling assumptions. To efficiently simulate the three-dimensional distribution of combustible gases under severe accident conditions, the HYCON3D code adopts the following assumptions.

• Low-Speed Compressible Flow

The containment flow is assumed to be low-speed compressible. In high-speed compressible flows, compressibility effects are typically associated with the conversion of kinetic energy into pressure energy and are characterized by the Mach number, often accompanied by shock wave formation. In contrast, during severe accidents in a closed containment building, pressure increases are primarily driven by mass and energy release rather than high-velocity flow phenomena. Therefore, conservation of mass and energy governs the pressure and density variations, which must be properly accounted for.

• Ideal Gas Equation of State

An ideal gas equation of state is employed. During severe accidents, the containment pressure may increase from atmospheric pressure (~1 bar) to the design pressure (~6 bar), while the gas temperature can exceed

100 °C. Within this range, the ideal gas assumption provides sufficient accuracy with significantly reduced computational cost compared to real gas models. Established containment analysis codes such as GASFLOW [6] and TONUS [7] also adopt the ideal gas assumption to enhance computational efficiency.

• Kinematic and Thermal Equilibrium Between Fog and Gas

When steam partial pressure exceeds the local saturation pressure, condensation occurs, forming fine droplets (fog) suspended in the atmosphere. The model assumes kinematic and thermal equilibrium between the gas and fog phases, meaning that both phases share the same velocity and temperature. This assumption enables efficient simulation of low-speed steam release jets while capturing the coupled thermo-fluid behavior.

The governing equations for the multicomponent gas mixture consist of the overall mass conservation equation, momentum conservation equation, energy conservation equation, and species mass conservation equations. For microscale condensation droplets, thermal and kinematic equilibrium with the gas phase is assumed; therefore, only the mass conservation of the condensed phase is explicitly solved. Under these assumptions, the governing equations are expressed as Eqs. (1)–(4).

$$\frac{\partial \rho}{\partial t} + \nabla \cdot (\rho \boldsymbol{U}) = S_\rho \tag{1}$$

$$\frac{\partial}{\partial t}(\rho \boldsymbol{U}) + \nabla \cdot (\rho \boldsymbol{U}\boldsymbol{U}) - \nabla \cdot \boldsymbol{R} = -\nabla \mathrm{p} + \rho \boldsymbol{g} + \boldsymbol{S}_m \tag{2}$$

$$\frac{\partial}{\partial t}(\rho Y_i) + \nabla \cdot (\rho Y_i \boldsymbol{U}) - \nabla \cdot \boldsymbol{J}_i = S_{Y_i} \tag{3}$$

$$\frac{\partial}{\partial t}(\rho h_s) + \nabla \cdot (\rho h_s \boldsymbol{U}) - \nabla \cdot \boldsymbol{q} = \frac{\partial p}{\partial t} - \left[\frac{\partial}{\partial t}(\rho K) + \nabla \cdot (\rho K \boldsymbol{U})\right] + S_h \tag{4}$$

The auxiliary transport terms appearing in these equations are defined as follows:

$$\boldsymbol{R} = 2\rho(\nu + \nu_t)\left[\dot{\boldsymbol{D}} - \tfrac{1}{3}(\nabla \cdot U)\boldsymbol{I}\right] - \tfrac{2}{3}\rho k \boldsymbol{I}$$

$$\boldsymbol{J}_i = \rho D_{im} \nabla Y_i - \rho Y_i \boldsymbol{V}_c + \rho \frac{\nu_t}{Sc_t} \nabla Y_i$$

$$\boldsymbol{q} = \rho \alpha_{\mathrm{eff}} \nabla \mathrm{h_s} + \sum_{\mathrm{i}} \mathrm{h_{si}} \left[\mathrm{J}_i + \left(\rho \frac{\nu_{\mathrm{t}}}{\mathrm{Sc_t}} - \rho \alpha_{\mathrm{eff}}\right) \nabla \mathrm{Y_i}\right]$$

Here, $\boldsymbol{R}$ is the effective stress tensor including molecular and turbulent contributions, $\boldsymbol{J}_i$ is the diffusive mass flux of species i, and $\boldsymbol{q}$ represents the total heat flux accounting for molecular and turbulent transport effects.

The mass fraction of fog generated by steam condensation is defined as the ratio of the fog mass to the gas mass, rather than the ratio of the fog mass to the total mass of the fog–gas mixture.

$$\alpha = \frac{m_f}{m_g} \tag{5}$$

$$\frac{\partial}{\partial t}(\rho_g \alpha) + \nabla(\rho_g \boldsymbol{U} \alpha) - \nabla(\Gamma_t \nabla \alpha) = S_\alpha \tag{6}$$

Eq. (6) represents the mass transport equation for the fog phase, where S_α denotes the mass generation rate due to steam condensation and fog evaporation.

3. CO Recombination by PAR

During a severe accident, reactor vessel failure may result in the discharge of molten corium into the reactor cavity, followed by molten corium–concrete interaction (MCCI). Depending on the concrete composition, MCCI can generate a significant amount of CO, which is a combustible gas.

Various studies have been conducted to investigate the control of CO using PARs. Earlier research primarily focused on catalyst poisoning effects, in which CO adsorption on the catalyst surface inhibits catalytic reactions. More recently, attention has shifted toward the recombination characteristics of CO during the late phase of severe accidents. It has been reported that when the catalyst temperature is elevated due to exothermic hydrogen recombination, the poisoning effect of CO becomes negligible.

Representative experimental programs investigating catalytic recombination of hydrogen and CO include the THAI HR-51 and HR-52 tests [8]. In parallel, several modeling approaches for CO recombination by PARs have been proposed, including (1) modified hydrogen recombination correlations, (2) detailed catalytic chemical kinetics models, and (3) mass-diffusion-based models.

The HYCON3D code incorporates a CO recombination analysis module (coPAR) based on a mass-diffusion-controlled approach. The chemical reaction for CO oxidation is expressed as

$$CO + \tfrac{1}{2} O_2 \Rightarrow CO_2 + 10\ MJ/kg \tag{7}$$

The catalytic recombination rates of hydrogen and CO are determined by their respective mass diffusion fluxes:

$$\phi_{H_2} = \rho h_{m,H_2} Y_{H_2} \tag{8}$$

$$\phi_{CO} = \rho h_{m,\mathrm{CO}} Y_{CO} \tag{9}$$

$$\phi_{O_2} = \rho h_{m,O_2} Y_{O_2} \tag{10}$$

The gas-phase mass transfer coefficient h_m is obtained from the Sherwood number correlation. Equations for hydrogen and CO recombination are valid under oxygen-sufficient conditions. However, during accident progression, oxygen concentration continuously decreases due to hydrogen recombination, potentially leading to oxygen starvation conditions.

Experimental results from the THAI [9] and THEMIS [10] projects have demonstrated that catalytic recombination efficiency (η) decreases under oxygen-deficient atmospheres. The oxygen surplus ratio Φ is defined as $\Phi = 2x_{O_2}/x_{H_2}$ or, when both hydrogen and CO are present, $\Phi = 2x_{O_2}/(x_{H_2} + x_{CO})$. The coPAR module adopts a smoothed linear function for the recombination efficiency depending on Φ:

$$\eta = max[0.6, min(1, 0.5\Phi)] \quad (11)$$

Under oxygen-sufficient conditions, the required oxygen consumption rate is determined from the stoichiometric ratio:

$$\dot{m}_{O_2,req} = \dot{m}_{O_2 byH_2} + \dot{m}_{O_2 byCO} = \frac{W_{O_2}}{2W_{H_2}}\dot{m}_{H_2} + \frac{W_{O_2}}{2W_{CO}}\dot{m}_{CO} \quad (12)$$

where W_i denotes the molecular weight of species i.

When the oxygen mass diffusion flux exceeds the required oxygen demand ($\dot{m}_{O_2} \geq \dot{m}_{O_2,req}$), the recombination rates of hydrogen and CO are expressed as

$$If\ \dot{m}_{O_2} \geq \dot{m}_{O_2,\mathrm{req}},\ \dot{R}_{CO} = \eta \cdot \dot{m}_{CO}$$
$$If\ \dot{m}_{O_2} \geq \dot{m}_{O_2,\mathrm{req}},\ \dot{R}_{H_2} = \eta \cdot \dot{m}_{H_2}$$

Under oxygen-deficient conditions, the recombination rates are limited by the available oxygen diffusion flux. In the present model, 20% of CO is preferentially recombined first. Subsequently, hydrogen recombination occurs, and any remaining oxygen is used for additional CO recombination.

- Step 1

$$\dot{R}_{CO} = \eta \cdot min\left(\dot{m}_{O_2},\ 0.2 \times \dot{m}_{CO}\frac{W_{O_2}}{2W_{CO}}\right)\frac{2W_{CO}}{W_{O_2}}$$
$$\dot{R}_{CO,remained} = \dot{m}_{CO} - \dot{R}_{CO}$$
$$\dot{R}_{O_2,remained} = \dot{m}_{O_2} - \dot{R}_{CO}\frac{W_{O_2}}{2W_{CO}}$$
$$\dot{R}_{H_2} = min\left(\dot{m}_{H_2},\ \dot{R}_{O_2,remained}\frac{2W_{H_2}}{W_{O_2}}\right)$$

- Step 2

$$\dot{R}_{O_2,remained} \Leftarrow max\left(0, \dot{R}_{O_2,remained} - \dot{R}_{H_2}\frac{W_{O_2}}{2W_{H_2}}\right)$$
$$\dot{R}_{CO} \Leftarrow \dot{R}_{CO} + \eta \cdot min\left(\dot{R}_{O_2,remained},\ \dot{R}_{CO,remained}\frac{W_{O_2}}{2W_{CO}}\right)\frac{2W_{CO}}{W_{O_2}}$$

The resulting recombination rates are incorporated into the species transport equations as source terms:

$$S_{CO} = -\dot{R}_{CO}$$
$$S_{H_2} = -\dot{R}_{H_2}$$
$$S_{O_2} = -\frac{W_{O_2}}{2W_{CO}}\dot{R}_{CO} - \frac{W_{O_2}}{2W_{H_2}}\dot{R}_{H_2}$$
$$S_{H_2O} = \frac{W_{H_2O}}{W_{H_2}}\dot{R}_{H_2}$$
$$S_{CO_2} = \frac{W_{CO_2}}{W_{CO}}\dot{R}_{CO}$$

A three-dimensional simulation of the HR-51 experiment was performed using HYCON3D. The computational domain reproduced the experimental geometry as shown in Fig. 1, including the internal cylinder and PAR housing. The coPAR module, based on a gas-diffusion-controlled recombination model was used to predict recombination rates as a function of the diffusive mass transport toward the catalyst surface. Geometric parameters of the AREVA PAR were specified through the "parProperties" file [5].

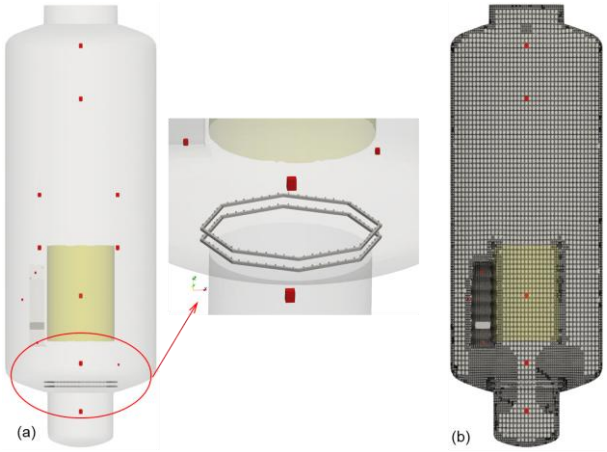

Fig. 1. (a) Geometry modeling of THAI test facility and gas sampling locations, (b) computational mesh for HR-51 test analysis.

For the energy equation, measured wall temperatures were imposed as time-dependent boundary conditions. The pressure vessel wall was divided into five patches (sumpWall, lowerWall, middleWall, upperWall, and headWall), each assigned the experimentally measured temperature history. Steam condensation at internal surfaces was modeled using the wall function-based wall-condensation boundary condition. The internal cylinder and PAR housing were treated as thin walls using a unsteady 1-D heat conduction boundary condition.

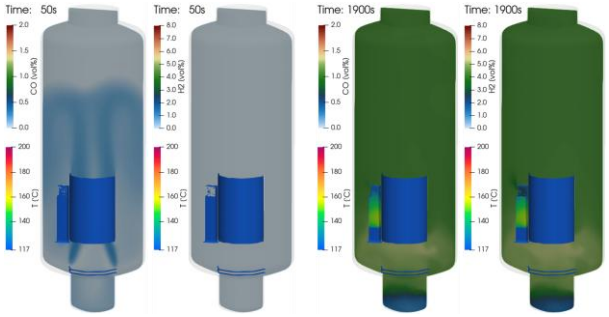

Fig. 2. Hydrogen and CO distributions at 50 s and 1900 s from the analysis results of the HR-51 test.

Fig. 2 presents the simulated distributions of hydrogen and carbon monoxide at 50 s and 1,900 s after the start of injection. At 50 s, CO injected from the upper nozzle ring rises along the internal cylinder toward the upper region of the vessel. At 1,900 s, elevated surface temperatures near the PAR housing indicate active catalytic recombination.

In Fig. 3, the predicted hydrogen concentration at the PAR inlet agrees well with the experimental data for both the first and second injection phases. As shown in Fig. 4, Similar agreement is observed for the CO concentration

at the PAR inlet, indicating that the transport and mixing behavior inside the vessel is properly captured.

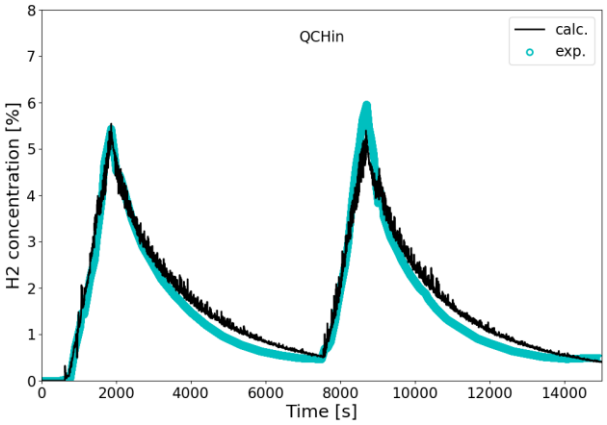

Fig. 3. Comparison of hydrogen concentration change over time at the PAR inlet.

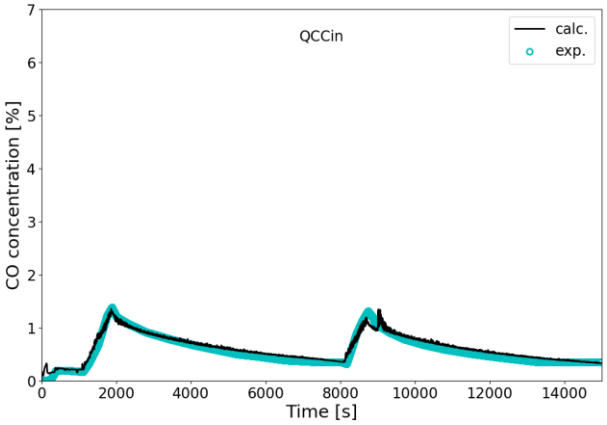

Fig. 4. Comparison of CO concentration change over time at the PAR inlet.

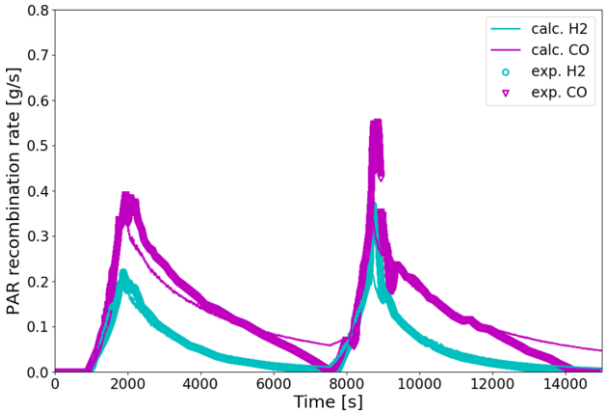

Fig. 5. Comparison of hydrogen and CO recombination rates for the HR-51 test.

Fig. 5 compares the calculated and measured recombination rates of hydrogen and CO. In the HR-51 test, CO was injected first, and hydrogen injection started approximately 600 s later. Under ambient temperature conditions, catalytic activity is delayed due to CO poisoning effects. Both the experiment and simulation show that catalytic recombination becomes significant only after hydrogen injection raises the catalyst temperature. The simulation successfully reproduces the initial activation characteristics of the PAR.

The predicted pressure evolution inside the vessel is also compared with experimental data at Fig. 6. The overall pressure trend follows the recombination rates of hydrogen and CO. Although the experiment exhibits a sharp pressure increase due to spontaneous ignition during the second injection phase, this phenomenon is not included in the present PAR model. Excluding the spontaneous ignition event, the model reasonably captures the pressure increase due to catalytic recombination as well as the pressure decrease resulting from wall heat losses and steam condensation.

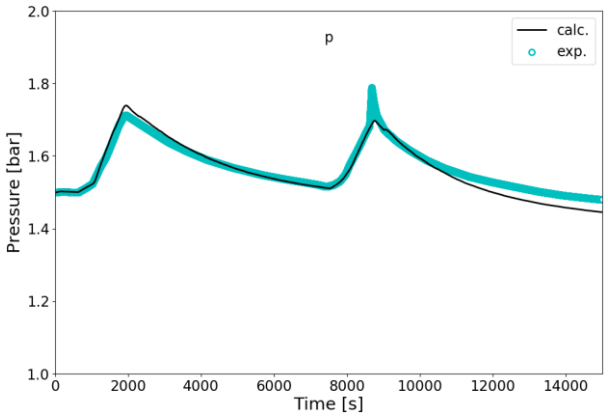

Fig. 6. Comparison of the vessel pressure change over time for the HR-51 test.

Overall, the comparison with the THAI HR-51 experiment demonstrates that the coPAR model accurately reproduces the catalytic recombination behavior of hydrogen and CO, including the initial activation delay caused by CO poisoning.

4. Application to the Korean typical high-power reactor containment Containment Analysis

According to domestic regulatory requirements for hydrogen control, the hydrogen distribution and safety within the containment were evaluated under the assumption of 100% metal–water reaction (MWR) of the active core in ref. [2]. As the severe accident progresses and the reactor vessel fails, molten corium relocates into the reactor cavity, where MCCI may occur. If the coolability of the relocated corium is not ensured during MCCI, continuous oxidation reactions may occur, potentially exceeding the hydrogen generation corresponding to 100% MWR of the active core.

The amount and composition of combustible gases generated during MCCI depend strongly on the concrete composition. Basaltic-type concrete contains relatively higher water content compared to CO_2, leading to increased hydrogen generation through MWR. In contrast, limestone common sand (LCS) concrete contains higher CO_2 content, resulting in increased carbon monoxide (CO) production.

Since the progression of severe accidents such as station blackout (SBO) can significantly influence

combustible gas generation depending on operator intervention, accident management actions, and concrete composition, a MELCOR analysis was performed under the following assumptions:

- Reactor cavity concrete: Limestone common sand
- Reactor cavity flooded
- Three-way valve depressurization from IRWST to steam generator compartment upon entry into severe accident management
- Well-spreading of corium on the reactor cavity floor
- Post-flooding of the reactor cavity
- Accident progression simulated up to 100,000 s (~28 hours) without operator intervention

Table I summarizes the major event timings obtained from MELCOR 1.86 analysis for an SBO accident of the Korean typical high-power plant.

Table I: MELCOR analysis results for SBO accident progression

Key event timings of SBO accident	
Event	Timing (s)
SBO initiation	0
pressurizer valve open	5,525
Start of core uncovery	7,562
SAMG entry condition	8,590
Start of core oxidation	8,590
Full core uncovery	8,767
Core support plate failure	9,249
Reactor vessel failure	12,713

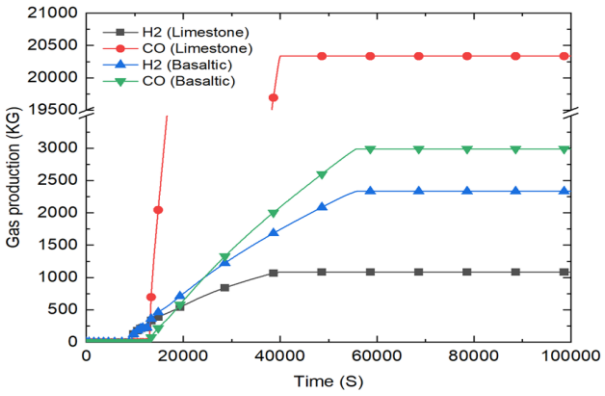

Fig. 7. Gas production rates by MCCI in the reactor cavity during the SBO accident.

The comparison of combustible gas generation for different concrete compositions (Fig. 7) indicates that LCS concrete produces significantly more CO and less hydrogen than basaltic concrete. However, when expressed in terms of hydrogen-equivalent moles (considering the molecular weight ratio of H2 to CO as 2:28), the total hydrogen-equivalent generation is approximately 1,250 kmol-H2, corresponding to about 2,500 kg-H2. This amount is equivalent to approximately 2.5 times the hydrogen generation under the 100% active core MWR assumption. The comparable hydrogen-equivalent generation predicted by MELCOR for different concrete types is attributed to modeling assumptions and accident management conditions.

HYCON3D simulations were performed using the time-dependent release rates of steam, hydrogen, and CO obtained from the MELCOR analysis. The simulation period extended from the onset of severe accident conditions to 100,000 s, incorporating both in-vessel MWR and ex-vessel MCCI effects.

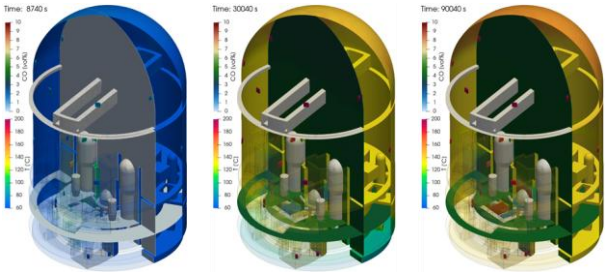

Fig. 8. CO distributions in the containment during the SBO accident.

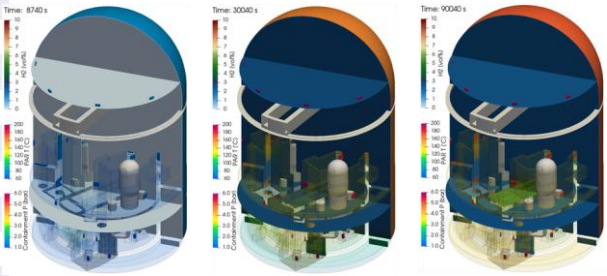

Fig. 9. Hydrogen distributions in the containment during the SBO accident.

Fig. 8 shows the temporal evolution of CO concentration distribution inside the containment. CO is released from the reactor cavity located at the lowest elevation of the containment and gradually disperses throughout the containment while mixing with the atmosphere. At approximately 30,000 s, the CO concentration becomes relatively uniform at around 5% due to significant steam dilution. At 90,000 s, higher CO concentrations (approximately 10%) are observed in compartments connected to the reactor cavity, such as the corium chamber region.

Fig. 9 presents the hydrogen concentration distribution. At 90,000 s, hydrogen generated by MCCI results in concentrations of approximately 6% in lower compartments, while the upper containment region, including the dome, shows concentrations of about 2%.

Figs. 10, 11, and 12 compare the total generated mass and the remaining inventory of hydrogen, CO, and steam within the containment. Hydrogen generation increases until approximately 40,000 s due to ongoing MCCI. Thereafter, the hydrogen inventory inside the containment gradually decreases as PARs operate. A similar decreasing trend is observed for CO inventory, indicating the effectiveness of PAR recombination. Steam generation continues due to boiling of coolant over relocated corium in the reactor cavity. However, after approximately 40,000 s, the total steam mass inside

the containment remains nearly constant due to condensation at containment walls.

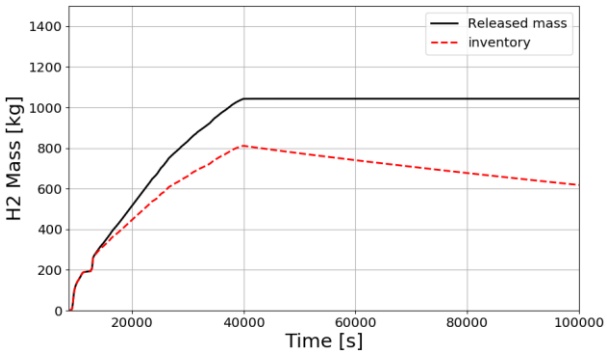

Fig. 10. Hydrogen mass inventory in the containment during the SBO accident.

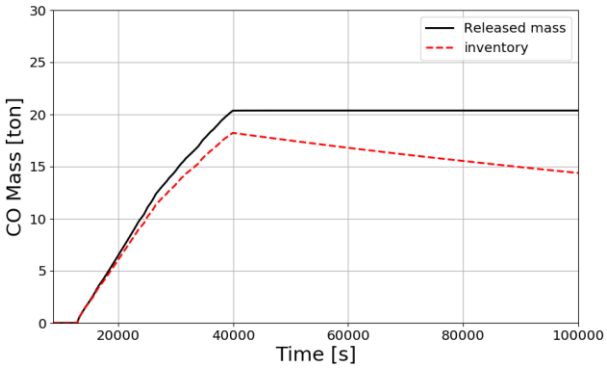

Fig. 11. CO mass inventory in the containment during the SBO accident.

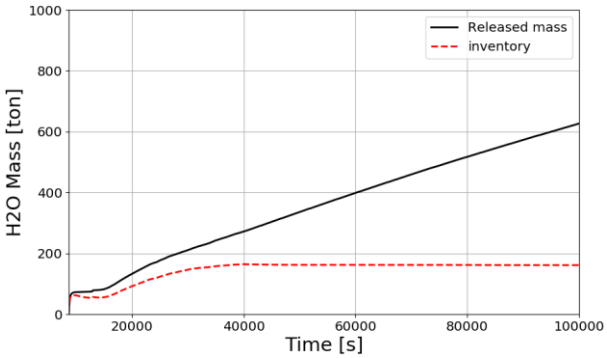

Fig. 12. Water vapor generation vs. mass inventory in the containment during the SBO accident.

Fig. 13 shows the containment pressure evolution. The pressure increases until approximately 40,000 s and stabilizes around 5 bar, indicating that non-condensable gas generation is the dominant contributor to pressure rise. Fig. 14 and 15 present gas concentration changes in the reactor cavity upper compartment (PAR-6 location) and containment dome region (PAR-30 location), while Fig. 16 shows the spatially averaged gas concentrations. Until approximately 20,000 s, steam concentration remains below 60%, indicating a potentially flammable condition. However, the overall concentration levels are insufficient to induce global detonation. After 20,000 s, steam concentration increases to approximately 70% and maintains a non-flammable condition up to 100,000 s.

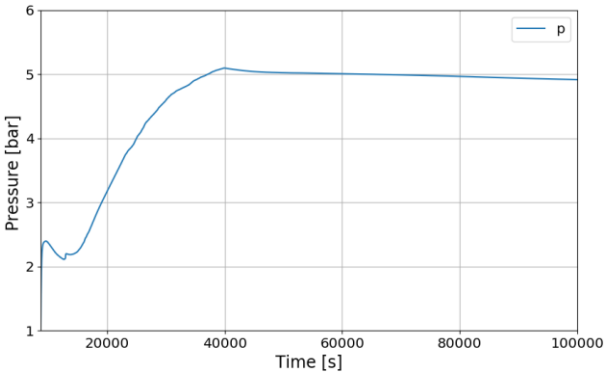

Fig. 13. Pressure change over time in the containment during the SBO accident.

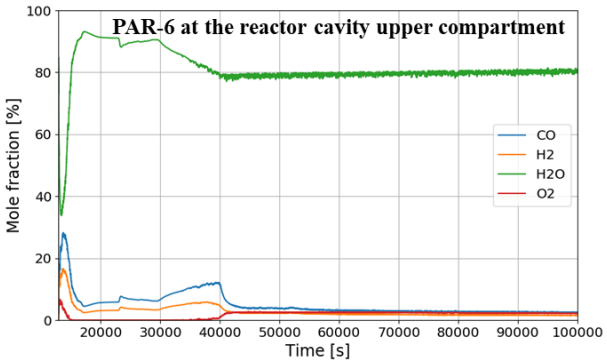

Fig. 14. Gas concentrations at the upper compartment of the reactor cavity in the containment during the SBO accident.

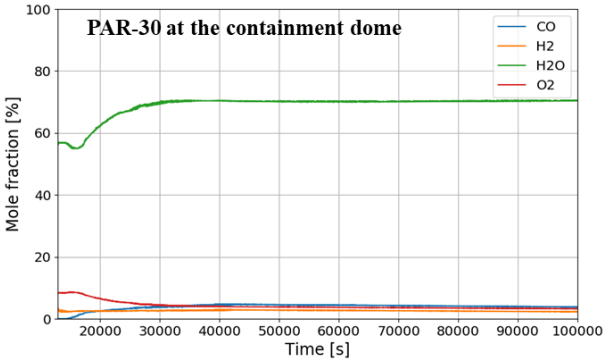

Fig. 15. Gas concentrations at the dome of the containment during the SBO accident.

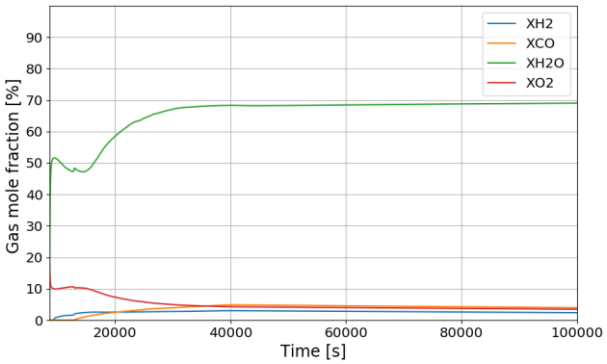

Fig. 16. Mean gas concentrations in the containment during the SBO accident.

Fig. 17 illustrates the hydrogen and CO removal rates by PARs installed in the containment. Until

approximately 40,000 s, combustible gases are continuously generated by MWR and MCCI, leading to a rapid increase in PAR recombination rates followed by gradual decline. Afterward, the increasing steam concentration reduces oxygen availability, resulting in decreased recombination rates for both hydrogen and CO.

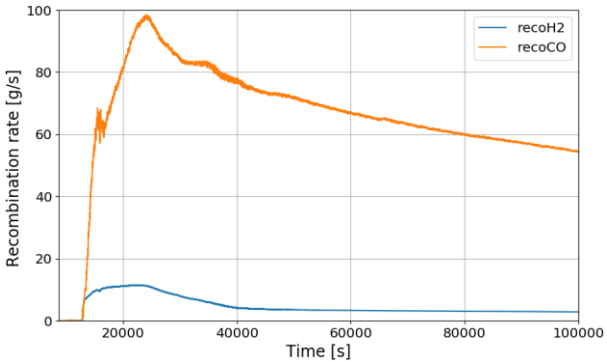

Fig. 17. Hydrogen and CO recombination rates by PARs in the containment during the SBO accident.

A ternary diagram, which represents the concentrations of flammable gases (including hydrogen and CO), air, and inert gases (such as steam and CO_2) on three axes, serves as a vital tool for visualizing the combustion characteristics of flammable gases within the containment during accident progression. Fig. 18 illustrates the ternary diagram showing the combustion characteristics of the atmosphere during the SBO accident in the Korean typical high-power plant. As the accident progresses, the containment atmosphere passes through the flammable region; however, it eventually transitions into a non-flammable (inert) state during the later stages of the accident due to the increased concentration of steam.

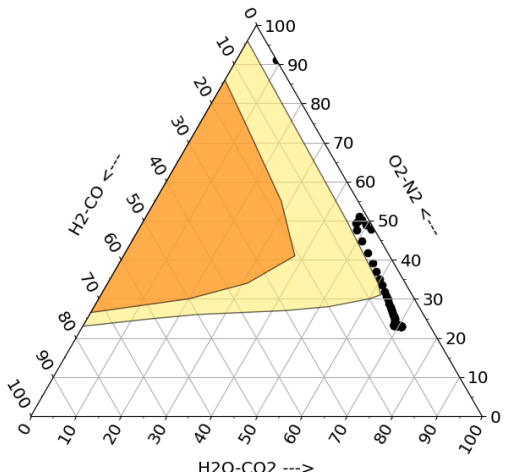

Fig. 18. Ternary diagram to show flammability of the mean gas concentrations in the containment during the SBO accident.

5. Summary and Future Works

HYCON3D, a detailed analysis code based on turbulence simulation, was developed to control flammable gases and assess their hazards within containment buildings under severe accident conditions. Furthermore, it introduces the mitigation of carbon monoxide to reflect the molten corium concrete interaction (MCCI) phenomenon in the late stages of severe accidents, which is currently being studied through the European AMHYCO project [11].

To evaluate the applicability of HYCON3D, we performed 3D analysis of the flammable gas distribution within the containment building during the early and late-phase SBO accident.

Currently, domestically manufactured PARs are installed in operating nuclear power plants in Korea. The coPAR model incorporated in HYCON3D is based on the diffusion rate of gas species; therefore, it can be applied not only to hydrogen recombination but also to CO recombination, regardless of the PAR type. Through analytical studies on a domestic PAR, it was confirmed that this diffusion-based PAR model exhibits hydrogen removal characteristics consistent with those predicted by correlation-based models. However, in order to apply this model under various accident conditions, experimental investigations on the recombination characteristics of mixed gases containing hydrogen and CO for the domestic PAR, as well as validation of the analytical model, are required.

To extend Severe Accident Management Guidelines (SAMGs), including combustible gas control, to the late phase of severe accidents, research findings on the combustion characteristics of flammable gases containing hydrogen and carbon monoxide are necessary. As a severe accident progresses into the late phase, the operation of PARs (or igniters) leads to hydrogen–oxygen recombination, which reduces the oxygen concentration in the containment atmosphere. Consequently, the oxygen-to-nitrogen ratio in air (21:79) changes, limiting the applicability of the Shapiro diagram. Bentaib et al [12]. proposed a new diagram for evaluating the flammability limits and deflagration-to-detonation transition (DDT) conditions of hydrogen–carbon monoxide mixtures. However, since air was used as the oxidizer in that diagram, it is difficult to directly apply it to evaluate combustible gas combustion characteristics under late-phase severe accident containment atmospheric conditions. A ternary diagram applicable to late-phase severe accident containment atmospheres should consist of three axes: (1) the concentration of flammable gases (hydrogen + CO), (2) inert gases (nitrogen + carbon dioxide + steam), and (3) oxygen. Experimental and/or analytical studies are required to support the development and validation of such a diagram.

ACKNOWLEDGMENTS

This work was supported by the Nuclear Safety Research Program through the Korea Foundation of Nuclear Safety (KoFONS) using the financial resource granted by the Nuclear Safety and Security Commission (NSSC) of the Republic of Korea. (RS-2021-KN063410).

REFERENCES

[1] J. Kim, H.T. Kim, D. Kim, “ Validation and Application of a Code for 3-D Analysis of Hydrogen Behavior during Severe Accidents”, Transactions of the Korean Nuclear Society Spring Meeting Jeju, Korea, May 18-19, 2023.
[2] J. Kim, K. Lim, “ Validation and Application of a Code for 3-Dimensional Analysis of Hydrogen-Steam Behavior in a Nuclear Reactor Containment during Severe Accidents”, Appl. Sci. 2024, 14, 15. https://doi.org/10.3390/app14156695.
[3] Frammatome, http://www.frammatome.com/solutions-portfolio/product/a0640, 2025.
[4] L.L. Humphries, B.A. Beeny, F. Gelbard, D.L. Louie, J. Phillips, “MELCOR Computer Code Manuals Vol. 1: Primer and Users’ Guide Version 2.2”, USNRC, 2017.
[5] J. Kim, K. Lim, Establishment of a computer analysis system for 3D hydrogen distribution in a containment building during a severe accident, KINS/HR-2114, 2025.
[6] J.R. Travis, P. Royl, J. Xiao, G.A. Necker, R. Redlinger, J. W. Spore, K.L. Lam, T.L. Wilson, C. Müller, B.D. Nichols, GASFLOW: A Computational Fluid Dynamics Code for Gases Aerosols, and Combustion VOLUME 1 Theory and Computational Model, KIT, 2011.
[7] S. Kudriakov, F. Dabbene, E. Studer, A. Beccantini, J.P. Magnaud, H. Paillere, A. Bentaib, A. Bleyer, J. Malet, C. Caroli, “The TONUS CFD Code for Hydrogen Risk Analysis: Physical Models, Numerical Schemes and Validation Matrix”, Nuclear Eng. and Design 2008, 238, 551–565; doi:10.1016/ j.nucengdes.2007.02.048.
[8] M. Freitag , B. von Laufenberg, M. Colombet, M. Klauck, "Measurements of the impact of carbon monoxide on the performance of passive autocatalytic recombiners at containment-typical conditions in the THAI facility", Annals of Nuclear Energy 141,107356, 2020.
[9] T. Kanzleiter, S. Gupta, K. Fischer, G. Ahrens, G. Langer, A. Kühnel, G. Poss, G. Langrock, F. Funke, Hydrogen and Fission Product Issues Relevant for Containment Safety Assessment under Severe Accident Conditions, Reactor Safety Research Project, 1501326 (2010), OECD-NEA THAI Project.
[10] M. Freitag, E. Schmidt, H. Nowack, PAR performance behaviour in H2-CO containing atmosphere Test HR-57, Comparison Report No. 150 1613 – CR – HR-57 DRAFT, 2022.
[11] J. Gonzalo, A. Bentaib, H.L. Enrique, N. Chaumeix, S. Kelm, et al.. AMHYCO Project overview and first outcomes. The 11th European Review Meeting on Severe Accident Research (ERMSAR2024), May 2024, Stochholm, Sweden. IRSN-04858153, https://asnr.hal.science/irsn-04858153v1.
[12] A. Bentaib, N. Meynet, A. Bleyer, "Overview on hydrogen risk research and development activities: Methodology and open issues", Nuclear Engineering and Technology, Vol.47, Issue 1, pp. 26-32, 2015.